Effect of Microstructure and Rare Earth Doping on Superconducting Properties of MgB_2 Bulk Processed by Spark Plasma Sintering

By

SUJOY GHOSH

THESIS

Submitted in partial satisfaction of the requirements for the degree of

MASTER OF SCIENCE

in

Materials Science and Engineering

in the

OFFICE OF GRADUATE STUDIES

of the

UNIVERSITY OF CALIFORNIA

DAVIS

Approved:

Prof. Subhash Risbud, Chair

Prof. Klaus van Benthem

Prof. Sabyasachi Sen

Committee in Charge

2021

Abstract

Spark Plasma Sintering is one of the most effective tools in modern sintering history. Since the discovery of superconductivity in MgB_2, there has been great interest in this atmospheric pressure-based material. In this paper, the effect of sintering temperature on superconducting and microstructural properties of MgB_2 material has been studied. Four sintering temperatures between 900 to 1200^0C were tested for their Critical Temperature (T_C). 1000^0C sample was found to have the highest diamagnetism and T_C was found to saturate at 38K in 1100 and 1200^0C samples. Defect states and long-range order was found to be a major factor in superconducting properties of the material. The effect of 3% Rare Earth (RE) dopants Lanthanum and Yttrium on superconducting and crystal properties was also studied. Formation of secondary phases and an increase in T_C of MgB_2 by 0.1K with Y doping were reported. Also, a Support Vector Regression model was developed and tested for finding suitable dopants for the material by predicting T_C values. The mean error in the test data set and variable temperature followed by Yttrium and Lanthanum doping was found to be +-1.26K and +-0.25K, respectively.

Acknowledgments

Although this thesis publication lists me as the author, its realization has been made possible by the help and support of my colleagues and fellow students who were there with me during these trying pandemic times. First and foremost, I would like to thank my thesis advisor Prof. Subhash Risbud, for his constant support and motivation to take up challenging projects and come up with solutions for real-world engineering problems. It was an honor to work with someone with his knowledge and experience. His constant support with new ideas allowed me to explore challenging avenues in the field of materials engineering. I am grateful for having the opportunity to collaborate with Prof. Valentin Taufour on superconductivity experiments. His constant support and expertise in the field of superconductivity have been a major factor in the completion of this project. I would also like to thank Prof. Klaus van Benthem and Prof. Sabyasachi Sen for accepting my invitation to be on my thesis committee.

I am thankful for all the support I received from the staff at Thermal Technology, Santa Rosa for helping me with the fabrication requirements of the project. I am grateful for all the help that Dr. Greg Peterson provided with his valuable insights and fabrication experience. Another major contribution to my research was Rahim Romario Ullah in Prof. Taufor's group who helped me with the superconductivity measurements and provided valuable insights on the results. I would also like to thank Yiqing Xia, Isabella Mueller, Rahul Jangid, Jugal Mehta, Jinfeng Zhao, and other students at UC Davis who were there with me throughout this journey and provided me with valuable advice during my research. I would also like to thank the entire AMCaT and CNM2 staff for their support with characterization experiments. The training I received from Dr. Andrew Thron on microscopy tools was a valuable asset towards making this project a reality. Support

from Dr. William Doering for my optical experiments was also highly useful towards making this project a reality.

Last but not least I would also like to thank my family and friends for supporting me throughout this journey. I could not have achieved any of this without their constant support and motivation.

Table of Contents

Figures

1. Introduction

The first known instance of superconductivity was demonstrated by Heike Onnes [1]. While reducing the temperature of mercury using liquid helium which was made possible by him only a few years before this discovery, he noticed that the resistivity slowly decreased at the beginning but there was a sudden drop in resistivity at 4.2K which was later called the Critical Temperature (T_c). During the initial findings, Onnes assumed that the resistivity had only dropped to a very low temperature, but it was later concluded that the value was nearly zero. Although it must be understood that this zero state of resistivity is impossible to prove experimentally as modern experimental techniques still cannot detect resistivity to such great precision. This new resistivity was called the superconducting state of a material. For simple metals, if a current is induced inside a coil by a magnetic field, the current will decay in a fraction of a second. In the case of superconductors, it will take an exponentially long duration of operation inside the coil to observe the presence of any such change. Given its zero resistance properties, it was expected that it could be used for high magnetic field operations. Experiments in that direction proved that there is an upper limit to the magnetic field which affects the T_c as the superconductivity ceases above a very low Critical Magnetic Field (H_C) [2]. Similar effects were also observed for current (I_C) which is a consequence of the H_C based effect as the current passing through a conductor generates a magnetic field [3].

Since this discovery, more than 100 superconductors have been discovered for various other elements making this phenomenon a lot more widespread than what it was previously assumed to be. It is also found in different types of materials such as metal, semiconductors, oxides, and organic compounds [4], [5]. The superconducting conditions also vary depending on its

specific applications, like with pressure and light [6]. Such materials can exist in various forms such as single crystal or thin films making them suitable for a wide variety of applications. It is one of the few fields which started decades back and continues to have the same research momentum as it did during its initiation.

1.1. High Temperature Superconductors

The major challenges in the field of superconductivity arise from the exceedingly low values of temperature required for maintaining the superconducting properties and the low I_C limit in the superconducting state. Ever since the discovery of superconductivity in mercury the rate of growth in T_C was exceedingly slow. It was claimed that there must exist an upper limit on maximum attainable superconducting temperature of 20K which later turned out to be erroneous. Although discoveries were made in Cu and Fe-based superconductors at T_C of 133K and 100K, they did not exceed the limit as the mechanism for superconductivity was different from conventional superconductors [7], [8]. A landmark achievement in this regard was the discovery of superconductivity in H_3S at 203K and in LaH_{10} at 250K which is only 50K away from room temperature superconductivity [9], [10]. What made these discoveries different from the earlier superconductors was the high pressures of nearly 100 GPa at which these metallic states exist, and the mechanism is more in line with traditional superconductors. One of the major challenges with these discoveries is the fact that such high pressures are impractical for use in every day applications. Room temperature superconductors have gained widespread popularity for their potential to be used in high magnetic field-based systems. such as magnetic levitation and magnetic resonance imaging. Broadly superconductors can be characterized into two categories of Type I and Type II superconductors depending on their transition characteristics in a magnetic field [11]. Type I superconductors immediately lose their superconducting property on crossing their T_C.

Type II superconductors tend to have a region of intermediate superconductivity where the material possess a mixed state of normal and superconducting state. The superconducting and normal state limits for this mixed region are given by T_{C1} and T_{C2} respectively.

1.2. BCS Theory

One of the most popularly accepted theories for superconducting materials is based on the one proposed by Bardeen, Cooper, and Schrieffer in 1957 which is called the BCS theory [12]. Electrons in a lattice face resistance from the lattice atoms which are vibrating at a certain frequency. As shown in Fig. 1, at the superconducting temperature when an electron passes through a given set of atoms it attracts the surrounding atoms which leads to distortions in the structure. When more than one such electron is present in the lattice it forms a cooper pair with the other electrons and which move together in the lattice. The cooper pair is linked to the adjacent electrons through a distance called the coherence length. This lattice distortion and cooper pair interaction is called the electron-phonon interaction where the distortion created in the lattice behaves like a single particle or phonon. Such waves of distortion flow through the material and carry the electron pair or cooper pair clouds through the lattice with 0 resistance. In the event of an increase of temperature above T_C the cooper pairs are broken, and the material goes back to its normal state.

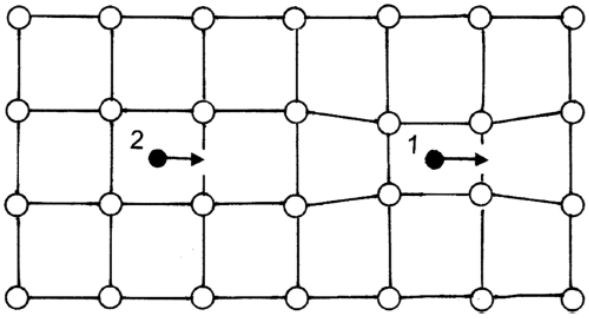

Figure 1: Electron Phonon interaction-based electron movement through lattice [13].

1.3. Magnesium Diboride

In 1994, a new era of superconductors came into existence which explored the development of intermetallic compounds doped with light atoms. Layered structures like cuprates were already known to have high superconducting temperatures which led to the possibility of MgB_2 being a strong candidate for a similar binary superconducting material. It was believed that the light atoms will increase the superconducting temperature by increased phonon vibrations [14]. One such material was MgB_2 which was discovered to have a very high superconducting temperature of nearly 39K [15]. This discovery led to a renewed interest in the material as it was considerably cheaper than the other standard room pressure-based materials such as copper-based superconductors which although had higher T_C, were costly to fabricate. MgB_2 can be fabricated in diverse forms ranging from bulk discs to thin films and wires, which made it practically viable for a wide range of applications [16]. The isotope effect and possibility for high Critical Current Density (J_C) also made it an interesting research topic [17]. As shown in Fig 2, MgB_2 has an AlB2 type structure with the Mg atoms forming the HCP lattice and the boron atoms lying on a plane at the center of the unit cell.

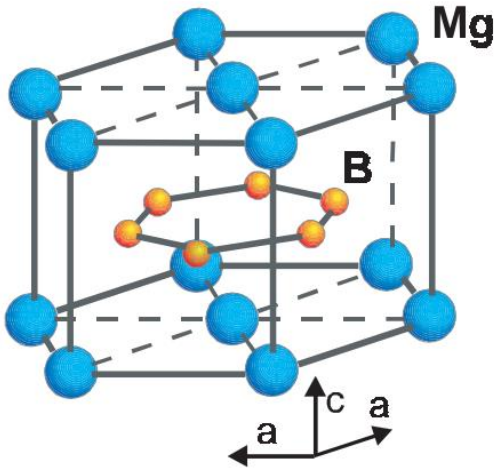

Figure 2: Layered AlB2 type crystal structure of MgB_2 [18].

This configuration of B atoms at the center allows for its superconducting properties which give a high T_C due to its c-a and a-a anisotropy. The unit cell is made up of B-B and Mg-B bonds. The B-B planes are considerably far apart which leads to weaker bonds between the atoms along the c axis as compared to a axis. There have been numerous other studies to find other borides with superconducting properties like MgB_2 but most of them have been found to have lower transition temperature than MgB_2 [19].

1.4. Problem Statement

The idea behind doping of MgB_2 arose from possible improvements in superconducting properties by the introduced dopant: (1) the new compounds formed could have improved T_C (2) the dopants could act as flux pinning centers, increasing the J_C in the superconducting state [20]. A dopant that marginally decreases the T_C can act as an effective flux pinning center due to lattice distortions created by the material. This in turn increases the J_C. In the past, numerous works have explored the effects of material properties on the superconducting properties of MgB_2 [21], [22]. Attempts have been made to substitute the Mg or B atoms with atoms of similar atomic size. It was initially expected that REs could be useful dopants to increase T_C as large atoms like La can change the lattice parameters which could lead to some interesting properties in MgB_2 [23]. Some RE elements in the form of pure metal and oxides have also been utilized as dopants for flux pinning applications which showed high J_C values owing to impurity scattering effects introduced by these dopants [24], [25]. Most of these sintering techniques are based on long durations of fabrication which tend to increase grain growth and reduce the long-range order observed in MgB_2 sintered materials, pivotal for its electron-phonon interaction. Most works on SPS based MgB_2 sintering focus on the consequent T_C and J_C values achieved by the dopants but not on the specific changes in materials composition and microstructure that lead to such behavior [26], [27]. Since maximum

densification is observed at 1200^0C, most work in this field has been limited by the decomposition temperature of MgB_2 in 1300 to 1600^0C range [28]. To date, very little is known about the change in lattice properties and its consequent effects on superconducting behavior at such high synthesis temperatures.

In this work, the effect of sintering temperature on superconducting properties has been studied. Lattice parameters were calculated and correlated to the superconducting properties. The effect of RE dopants on material crystal structure has also been explored and possible RE substitutions have been suggested. The effect of material microstructure on T_C has also been explored. The samples were characterized using Magnetic Property Measurement System (MPMS), Scanning Electron Microscopy (SEM), Energy Dispersive Spectroscopy (EDS), Transmission Electron Microscopy (TEM), and Xray Diffraction (XRD). Support Vector Regression tools were used to find the most promising dopants for MgB_2 materials processed by Spark Plasma Sintering based on lattice parameter calculation referenced with dopant experimental database obtained from the literature.

2. Experiment

2.1. Powder Preparation

MgB_2 powder of 100 mesh and 99% purity was acquired from Sigma Aldrich. Four different samples were prepared for sintering at 900, 1000, 1100, and 1200°C. Lanthanum (La) powder of 40 mesh and 99.9% purity were acquired from Sigma Aldrich. The powder was obtained pre-suspended in oil to prevent oxidation before sintering in the open air. For La-doped samples the MgB_2 powder was mixed with La suspension using mortar and pestle. Yttrium (Y) powder of 40 mesh and 99.5% purity was acquired from Sigma Aldrich and mixed with MgB_2 to obtain the Y doped samples. Most works in the past have attributed suitable flux pinning without majorly

reducing T_C to a RE dopant concentration of 3% by mass. Therefore, the La and Y doped samples were doped by a 3% mass concentration relative to MgB_2.

2.2. Spark Plasma Sintering

Spark Plasma Sintering (SPS) is a sintering technique that uses Joule heating in combination with a pressure to produce compact shapes for conductive materials. The basic design of the SPS setup is shown in Fig. 3 (a).

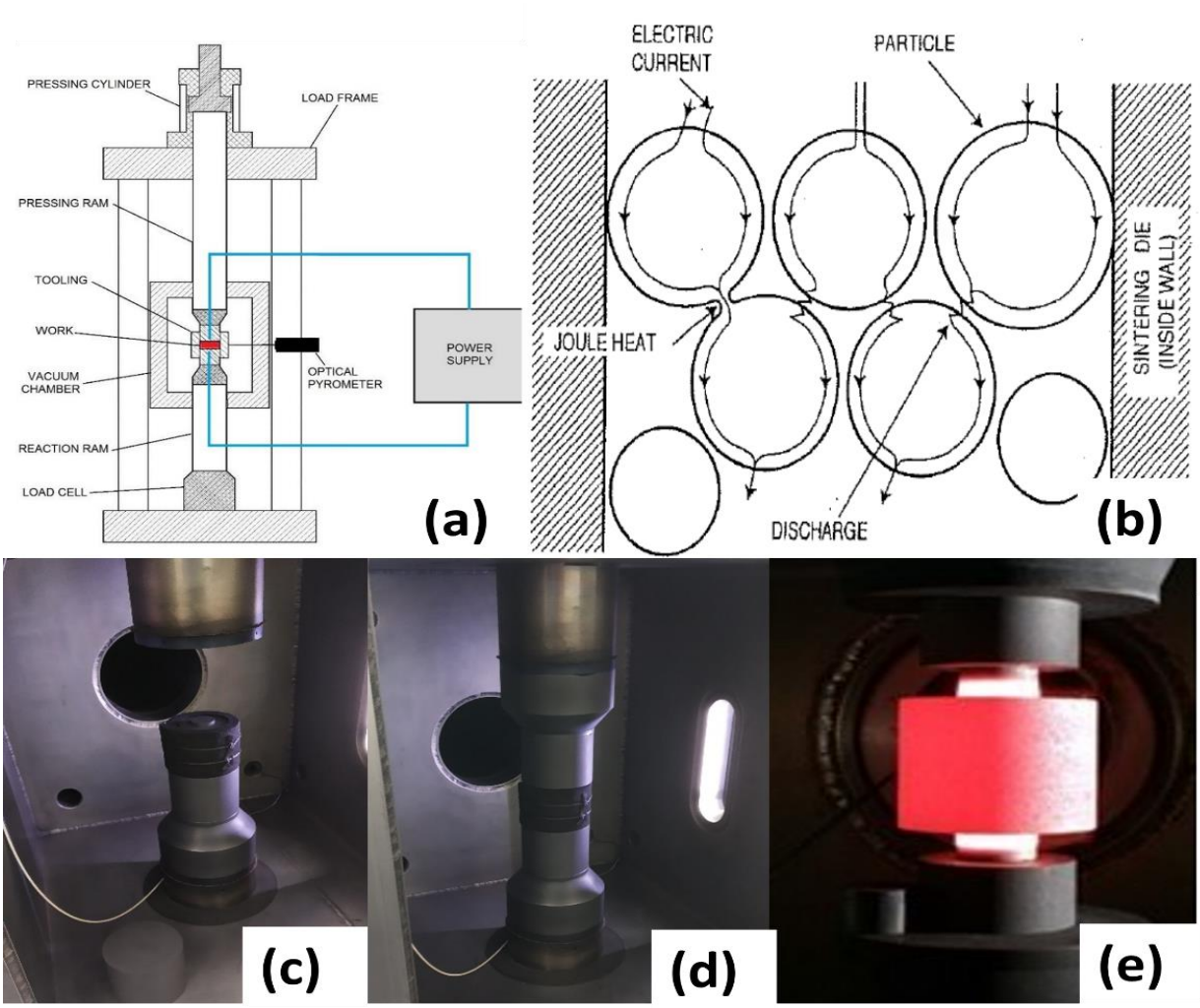

Figure 3: (a) Complete SPS setup (b) Neck formation during sintering (c) Sample placed in SPS chamber between the vertical pressing ram (d) Sample under 70 MPa uniaxial pressure (e) Depictive image of heat produced in the die during the experiment.

The powder is pressed between two arms which provide uniaxial force and a high pulsed or constant current is passed through the sample. Optical pyrometers are used to measure and control the sintering temperature. It is one of the best techniques for achieving maximum possible density in bulk materials due to the combined effect of uniaxial pressure and joule heating which is more effective than traditional hot press techniques. In hot presses, the heat is delivered from the top and bottom of the press and this leads to non-uniform heating at the center of the material. As shown in Fig. 3(b), this high current is delivered into the sample which produces joule heating in the grains of the material. As shown in Fig 3(c) & (d), the powder is placed between two graphite foil layered dies, enclosed in an insulating sleeve, which was kept between the pressing arms. As shown in Fig. 3(e), depicting the heating in the absence of an insulating sleeve, as the current is passed through the sample it heats the entire sample and the die to ensure uniform sintering of the sample. The heat produced inside the bulk is more uniform as individual particles generate their own heat by converting the current to heat energy leading to more effective necking between the individual grains. This greatly helps increase the speed of sintering and leads to reduced coarsening which is associated with longer heating and cooling time [29]. Although the name mentions Spark Plasma, it is still not conclusively known if sparks or plasma are generated during the sintering. The densification is mostly attributed to temperature-based vapor formation and pressure induced neck formation that leads to bonding between adjacent particles.

The sintering experiments for our samples have been developed with a Thermal Technology DCS 50 furnace. For maximum densification, constant uniaxial pressure of 70 MPa was utilized as beyond this value, negligible compression is observed. A current of 2000A at 4V was maintained in a 10^{-3} bar vacuum. Each sample was steadily heated for 20 mins at the required temperature and pressure in the Ar atmosphere.

2.3. Support Vector Regression

The lattice parameters in MgB_2 greatly contribute to its superconducting properties. Literature survey using machine learning which elucidates the change in these parameters with doping can be a useful tool for predicting superconducting properties of the system. Support Vector Machine (SVM) is a machine learning based supervised classification technique that attempts to classify data by breaking it into categories [30]. It is based on the VC theory that makes it a useful statistical tool for data analysis and regression [31]. As shown in Fig. 4(a) The model is first trained with a sample data set which is broken down into two categories with a hyperplane. The system aims to maximize the difference between the two categories. Depending on which region the data set lies in the sample space mapped by ∅, it is allocated a specific category in the same data space. As shown in Fig. 4(b), although this tool is mostly used as a classification method for binary results, it can also be evolved for solving nonlinear problems by mapping the data in a multidimension space.

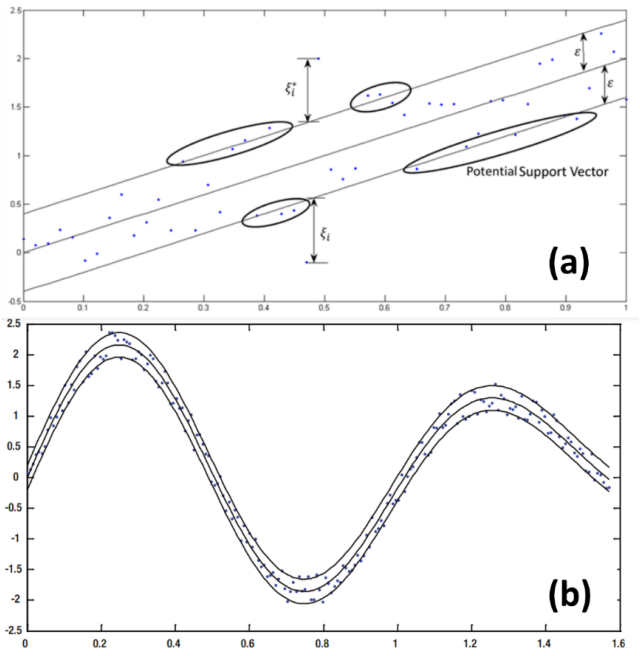

Figure 4: (a) Linear Support Vector Classification (b) Non-Linear Support Vector Classification.

Most regression models like Ordinary Least Squares try to reduce the error in data by drawing a linear/nonlinear curve and minimizing the square of error. Support Vector Regression (SVR) models provide the user with greater control over the output as the error margin can be chosen while designing the model. SVR focuses on reducing the coefficients of the model. The maximum error of the system is given by ε which decides the model coefficients.

$$Minimization\ function: Min(\frac{1}{2}w^T w + C\sum \varepsilon) \quad (1)$$

$$Polynomial\ Kernel: K(x,y) = (\ x^T\ y + \ \mathrm{C})^{\ d} \quad (2)$$

$$Training\ function: |w^T \emptyset(x) + b| \leq 1 - \varepsilon \quad (3)$$

Here:

y= Target

C= penalty parameter for the error term

w=normal vector to hyperplane

x= predictor

d=order of polynomial

One of the major challenges in choosing a suitable dopant for an experiment is understanding how a change in lattice parameters can affect the T_C over a wide range of dopants. We trained our model with a known data set of lattice parameters and T_C found in the literature [32]. Using the trained model, we tested the doped and undoped samples for the accuracy of predictions.

2.4. Superconducting Measurements

Small pieces of 5x2x2 mm were cut from the polished samples and used for T_C measurements. A Quantum Design Magnetic Property Measurement System (MPMS) was used to measure the

superconducting properties of the system. The samples were placed in Field Cooled with 20 Oe magnetic field for T_C measurement.

2.5. SEM-EDS and XRD

SEM and XRD samples were prepared by polishing using Silicon Carbide paper to remove the outer graphite foil. Small parts from the interior of the disc were cut and observed using an Olympus SZ61 optical stereoscope to check the consistency of material color and texture. High and low magnification SEM images were taken for each sample using the Thermo Fisher Quattro S Environmental SEM tool. The high magnification images were used for EDS analysis. XRD analysis was done using PANalytical X'Pert Pro MRD. Lattice parameters were calculated using Bragg's law for a hexagonal crystal. Crystallite size and strain were calculated using Williamson-Hall Plot [33].

2.6. TEM

Samples for TEM analysis need to be less than 100 nm in thickness as TEM images are produced by capturing transmitted waves of electrons which get absorbed at higher thickness. As shown in Fig. 5 (a) to (e), Ion beam milling tools are used to obtain a wedge-shaped sample with nearly 80 nm thickness on the surface of the disc. FIB was performed using FEI Scios DualBeam FIB/SEM. The wedge is then welded to a tungsten probe and an ion beam is used to cut the wedge out of the surface. The wedge is then lifted and placed on a grid and welded using tungsten.

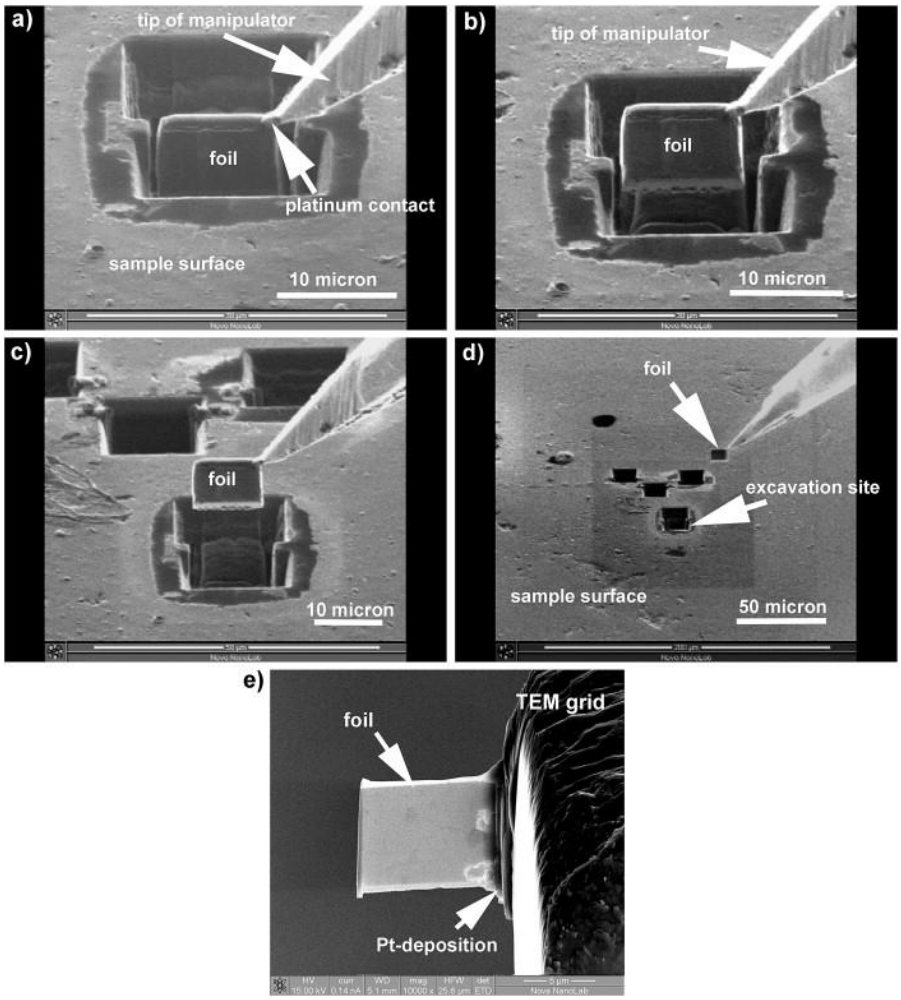

Figure 5: (a) Wedge is excavated (b) Wedge is soldered to probe (c) Wedge is removed from the sample (d) SEM image of sample site (e) Wedge is soldered to the grid [34].

The grid obtained from FIB is then used to observe the High-Resolution TEM (HR-TEM) pattern of the material with the JEOL JEM 2100F-AC TEM tool.

3. Results and Discussion

3.1. Effect of Synthesis Temperature

3.1.1. Color Anisotropy

Optical images of the bulk samples show a change in color with an increase in synthesis temperature. As shown in Fig 6., the color changes from dark grey to goldish black from 900 to 1200°C. The rigidity of the material was also found to be very low at 900°C which indicates that necking begins at temperatures 1000°C and above. Such optical properties can be explained by the c-a axis

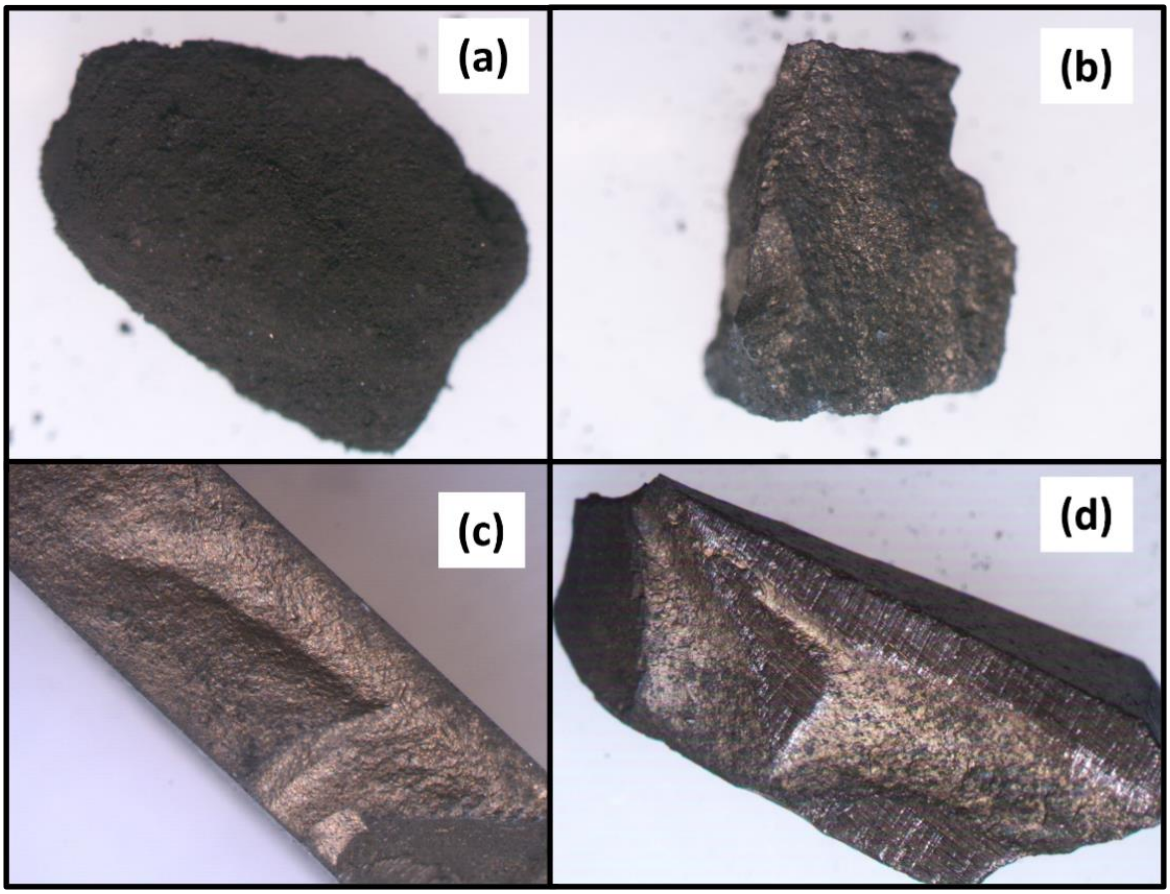

Figure 6: Color transition in optical images of samples developed at (a) 900 (b) 1000 (c) 1100 & (d) 1200°C.

anisotropy observed in MgB_2 crystals [35]. The lattice structure of MgB_2 is made up of an AlB2 type hexagonal unit cell. The MgB_2 has a structure similar to graphite where the adjacent atoms in the plane are bonded by strong sigma bonds and planes by weak pi bonds. The superconducting properties of MgB_2 are a result of its strong electron-phonon coupling in the B planes. These B-B bonds have strong electron-phonon interaction along with the sigma bonds and weak scattering along with the pi bonds. A very strong inter-band transition has been calculated to occur at 2.6 eV. The reflectivity plasma edges for a and c axis are nearly 2 and 2.5 eV which gives rise to interesting polarization properties. As polarization is rotated from the a to c axis the material color changes from dark grey to a golden tinge. The 2.5 eV inter-band transition is also seen in the case of gold material which explains why the color is golden for c axis polarization [36]. For polycrystalline samples like in Fig. 6, the resultant color is dependent on the average anisotropic optical properties of the material. The change in color from dark grey to golden black depends on the microstructure and lattice parameters of the material [37]. The impurity scattering function which depends on the defect states and substitutions also decides the overall color. The gold patterns are seen to increase in the material from 900 to 1100^0C and get darker again at 1200^0C. This could indicate a decrease in material defects and increase in lattice strain till 1100^0C followed by a reversal of properties on a further increase of temperature, indicating a limit on optimum sintering properties.

3.1.2. Effect on Superconductivity

Magnetic moment measurement using the MPMS was performed on all 4 samples. The onset of transition to superconducting state (T_{C2}) was found to occur at 39K. The superconducting state is defined as 90% of the material's 4K moment value. As given in Fig. 7(a), T_C for 900, 1000, 1100 & 1200°C were found to be 30, 37.8, 38 & 38K respectively. The 900°C sample was found to

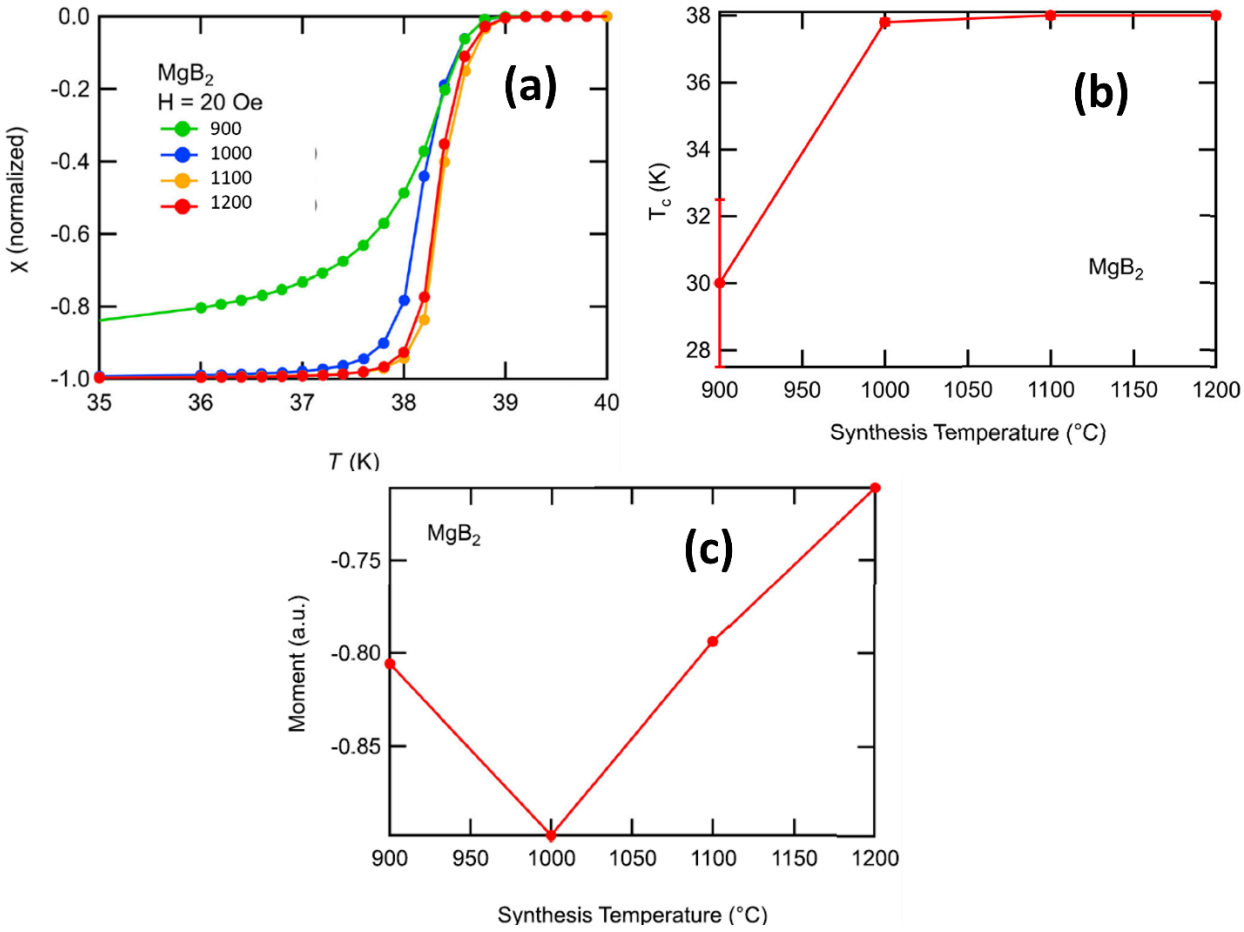

Figure 7: Magnetic moment showing T_C for different synthesis temperatures (b) T_C compared to synthesis temperature (c) Plot of T_C moment at T= 5K as a function of growth temperature showing 1000°C to have the largest diamagnetic signal.

have significantly larger intermediate zone between T_{C1} and T_{C2}. A general trend indicates a decrease in the intermediate zone with increasing temperature. This indicates that MgB_2 is a type II superconductor. As shown in Fig. 7(b), the T_C increases rapidly from 900 to 1000°C and then stabilizes to a constant value of 38K. This indicates an upper limit to T_C in MgB_2 powder processed with SPS. As shown in Fig. 7(c), comparing the diamagnetic signals from 4 samples, the sample developed at 1000°C shows the strongest signal indicating maximum expulsion of the magnetic field from the material obtained showing a strong Meissner effect [38]. The diamagnetism of a

superconductor depends on the screening currents generated in the material below T_C [39]. The screening current flows at a penetration depth of λ below the superconductor which in turn generates a magnetic field that opposes the actual field. This relationship, known as the London equation, only works if the coherence length $\xi << \lambda$. As compared to the other samples, the 1000^0C material would need to have the highest coherence length to get the highest diamagnetism. Type II superconductors have an intermediate zone which is made up of vortices arranged in a vortex lattice where the vortices are in a normal state, but the surrounding material is superconducting [40]. The J_C is the value beyond which the vortices are allowed to move which in turn reduces T_C. In 900^0C the large intermediate region indicates the presence of higher defect states which trap these vortices.

3.1.3. Material Structure

XRD scans for the samples were compared to understand the effect of synthesis temperature on crystal properties. As shown in Fig. 8, the primary phase was found to be MgB_2 which has a hexagonal structure with P6/mmm space group [41]. Secondary phases of MgO and MgB_4 were also present in the samples with space groups of Fm-3m and Pnma, respectively [42], [43]. It can be observed that with increasing temperature stronger peaks indicative of the MgB_4 phase are found to increase in the sample. One possible cause of the same could be the relatively lower atomic mass and size of the B atom that allows the atom to dislocate more during high-temperature operation. The initial (100) & (001) peak is also observed to increase in intensity with increasing temperature indicating a change in a and c axis lattice parameter, respectively. Overall, the peaks for the samples are observed to shift with temperature indicating a correlation of synthesis temperature with lattice parameters. Mg has strong affinity for oxygen, but MgO is a non-superconducting phase which acts as flux pinning center like other oxides. It is also similar in

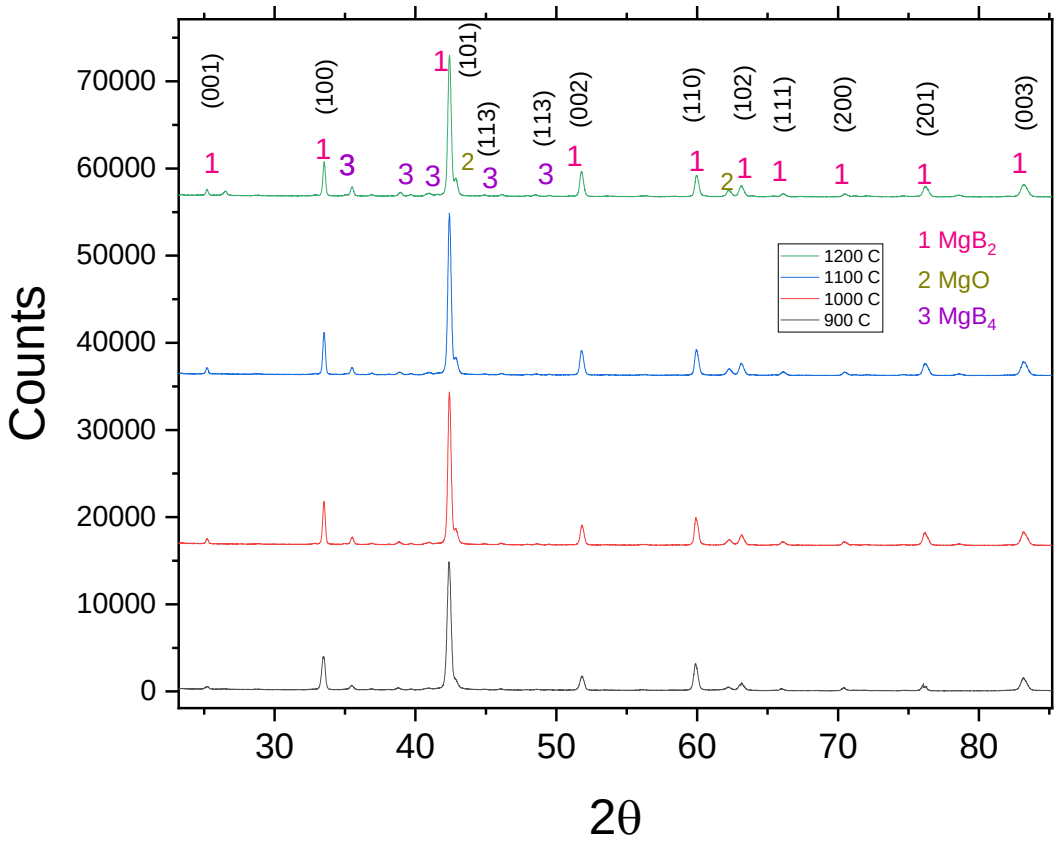

Figure 8: XRD scan at different synthesis temperatures showing the presence of (1) MgB_2 and secondary phases of (2) MgO and (3) MgB_4.

size and structure to MgB_2 because of which it appears as shoulder adjacent to MgB_2 peaks and it makes it easier for defects to be introduced by the phase in the lattice. It can form stacking faults between the layers of Mg and B.

Fig. 9(a) shows the calculated lattice parameter for increasing synthesis temperature. The a-axis parameters are observed to decrease in size indicating lattice compression along the Mg-Mg plane. The c axis parameters show an increasing trend till 1100^0C but are seen to decrease at 1200^0C. Indicating a general tendency of the lattice to expand along the 001 plane at higher temperatures and increasing interplanar spacing till 1100^0C. As in Fig. 9(b) the crystallite size

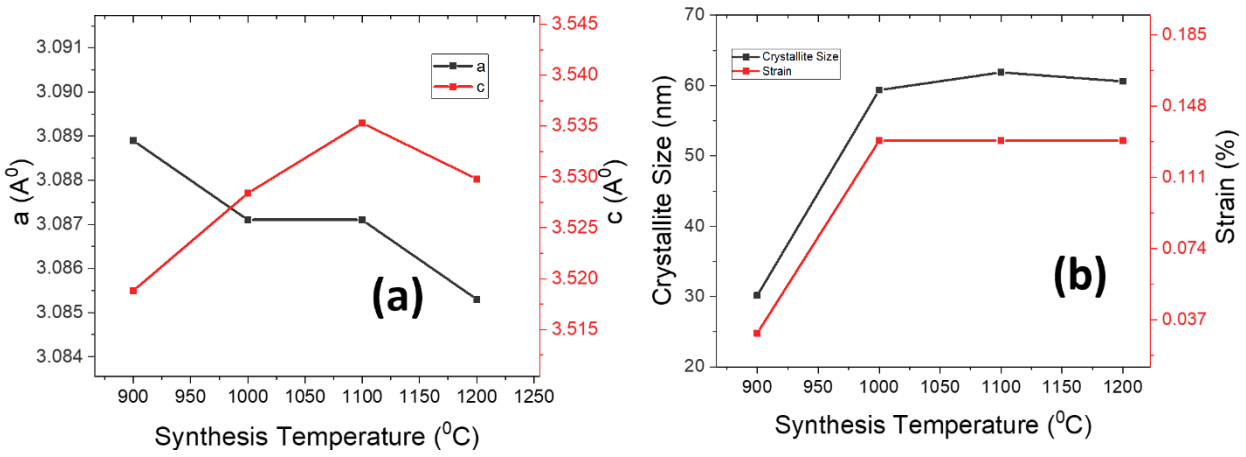

Figure 9: (a) Calculated lattice parameters from different synthesis temperatures (b) Crystallite size and strain for increasing synthesis temperature.

increased rapidly from 900 to 1000 and then started decreasing after 1100^0C. This could indicate the growth of a secondary phase such as MgB_4 which introduces lattice mismatch after 1100^0C. The defects introduced by MgB_4 can be seen in Fig. 10(a) & (b) which show the lattice mismatch introduced by the MgB_4 (114) plane in MgB_2 (101) matrix.

Similarly, there was a major change in strain from 900 to 1000^0C but the consequent lattice strain values were found to be relatively constant. The properties of MgB_2 at 900^0C are considerably poor as compared to the higher temperature value indicating higher porosity and lower necking behavior of the material. This inverse behavior of the c and a axis is an outcome of bond strength between the atoms. B-B bonds are stronger than Mg-B bonds which hold the lattice together. This leads to lattice distortion and strain in high temperature sintering.

With increasing strain, there is an increase in c axis and a decrease in a axis parameter. The T_C values of a material depend on the phonon frequency of the superconducting plane. In MgB_2, the superconducting plane is believed to B. It is evident from Fig. 9(a) that with the decrease of a axis lattice parameters the B-B and Mg-Mg sigma bonds are brought closer to each

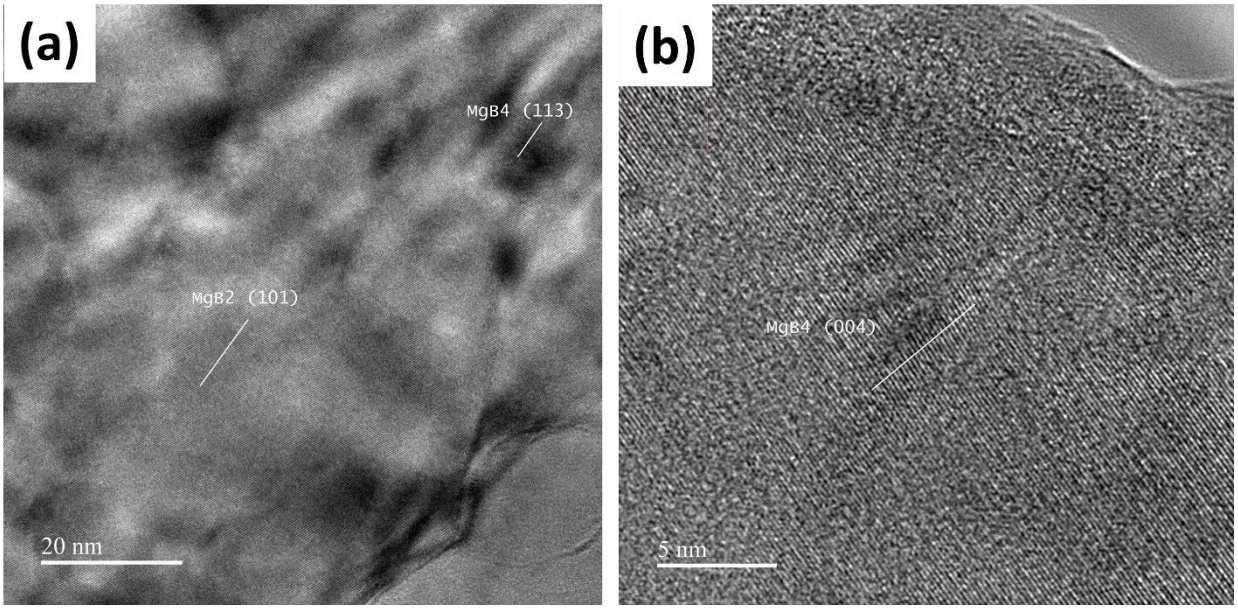

Figure 10: (a) HR-TEM surface lattice structure shows the secondary MgB_4 phase in MgB_2 primary phase. (b) Magnified (004) MgB_4 plane.

other but with the increase of c axis there is an increase in out of plane lattice vibration which is a result of weak bonding between Mg-B planes. The decrease in B-B bond length increases the in-plane electron-phonon interaction which increases T_C till 1100^0C.

The staturation of T_C at 1100^0C, decrease in c axis and crystallite size after 1100^0C can be understood with the SEM microstructure. Fig. 11 (a) to (d) shows smoother surface profile which indicates increasing necking from 900 to 1100^0C but beyond that value, grain growth starts occuring. Grain boundaries play an important role in superconducting behavior of MgB_2. The grain boundaries carry high transport currents as compared to other conventional high-T_C superconductors which form grain boundary weak links [44]. Due to weaker links the field required to penetrate the center of the grains is low which explains why the diamagnetism starts decreasing after 1000^0C. When temperature increases beyond 1100^0C the presence of mixed phases introduces weak links into the material and the grains decouple electronically at very high

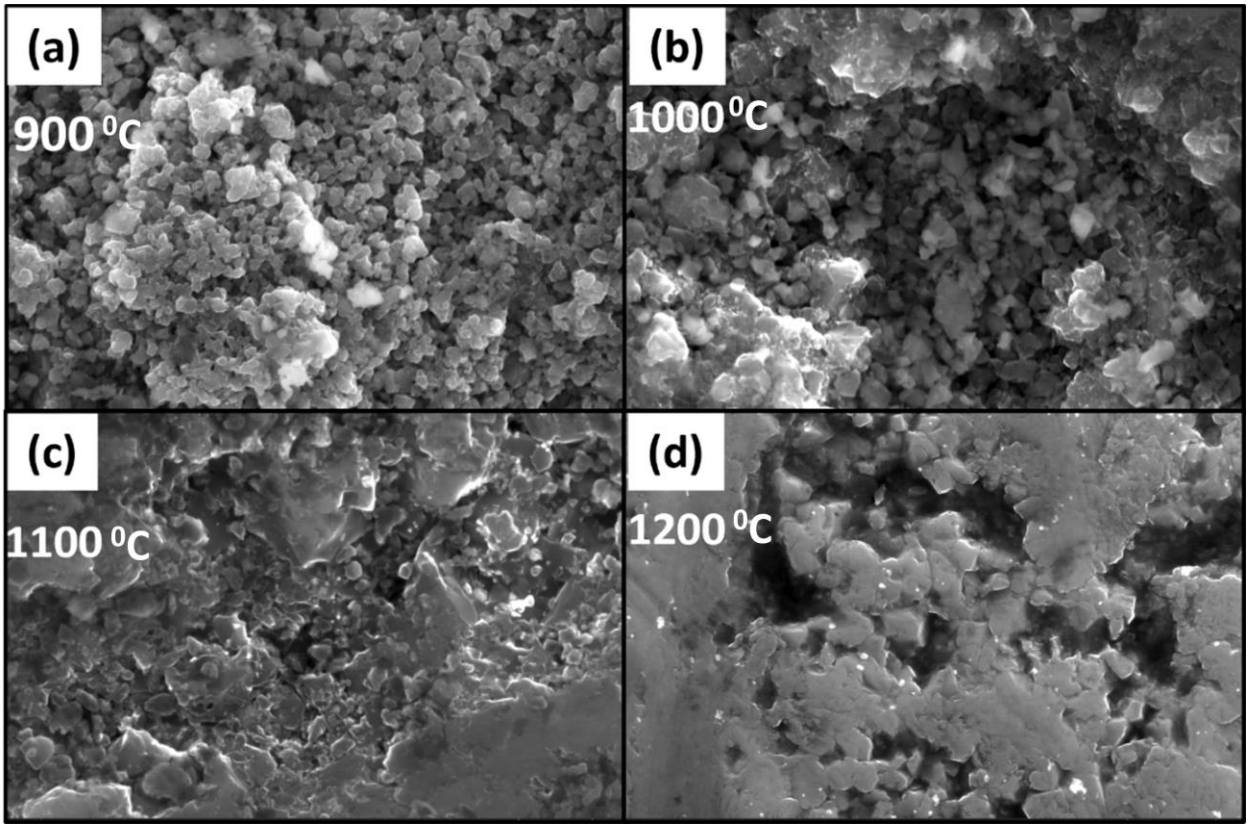

Figure 11: SEM particle morphology for different synthesis temperatures.

As shown in Fig. 12 (a) to (d), the EDS elemental color maps for the samples indicate more smoother surface texture with increasing synthesis temperature till 1100 followed by increased surface features at 1200^{0}C. Maps of 1000 and 1100^{0}C show an increase in dark patches leading to Mg deficient regions. The B map in these regions seems to have an increase in intensity. 1200^{0}C showcases segregation of the elements in Mg, O regions and a B dominated region. As observed previously in Fig. 8, this could imply the formation of the secondary phase MgB_4 and MgO in the microstructure. This could explain the increase in dark Mg pits observed from 1000 to 1100^{0}C as possible onset of segregation into Mg deficient and excess regions.

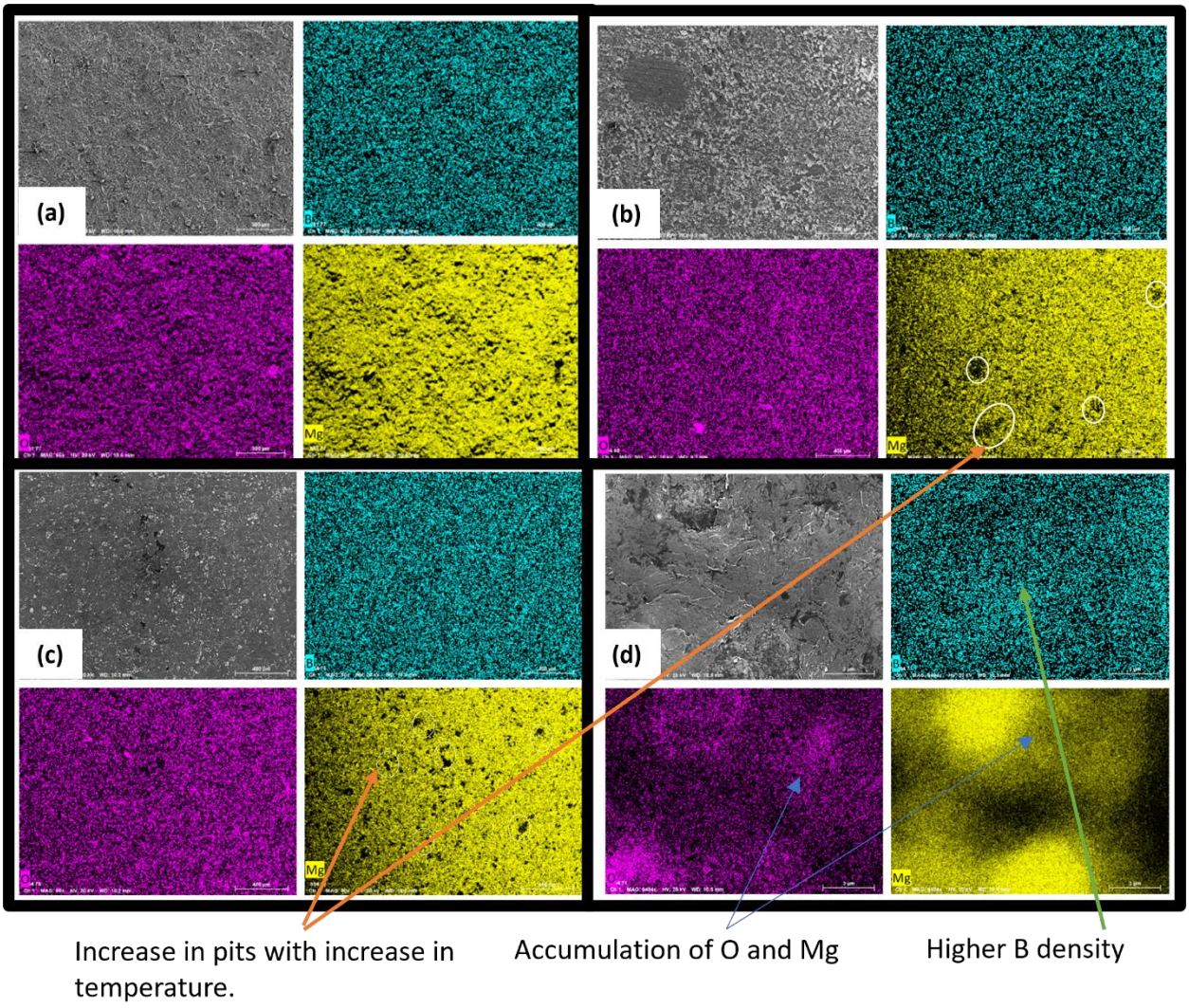

Figure 12: SEM-EDS color maps of Boron, Oxygen, and Magnesium distribution on disc surface at (a) 900 (b) 1000 (c) 1100 & (d) 1200^0C synthesis temperature.

The B atom is lightest amongst all the atoms present in the material. With the increase in sintering temperature, the maps shown an increase in MgB_4 and MgO phase which are non-superconducting phases. Therefore, the superconductivity in 1200^0C sample is a result of flux pinning and disorder introduced during sintering as the atomic bonds between MgB_2 are broken to allow formation of secondary phases.

3.2. Effect of Rare Earth Doping

3.2.1. SVR Dopant Choice

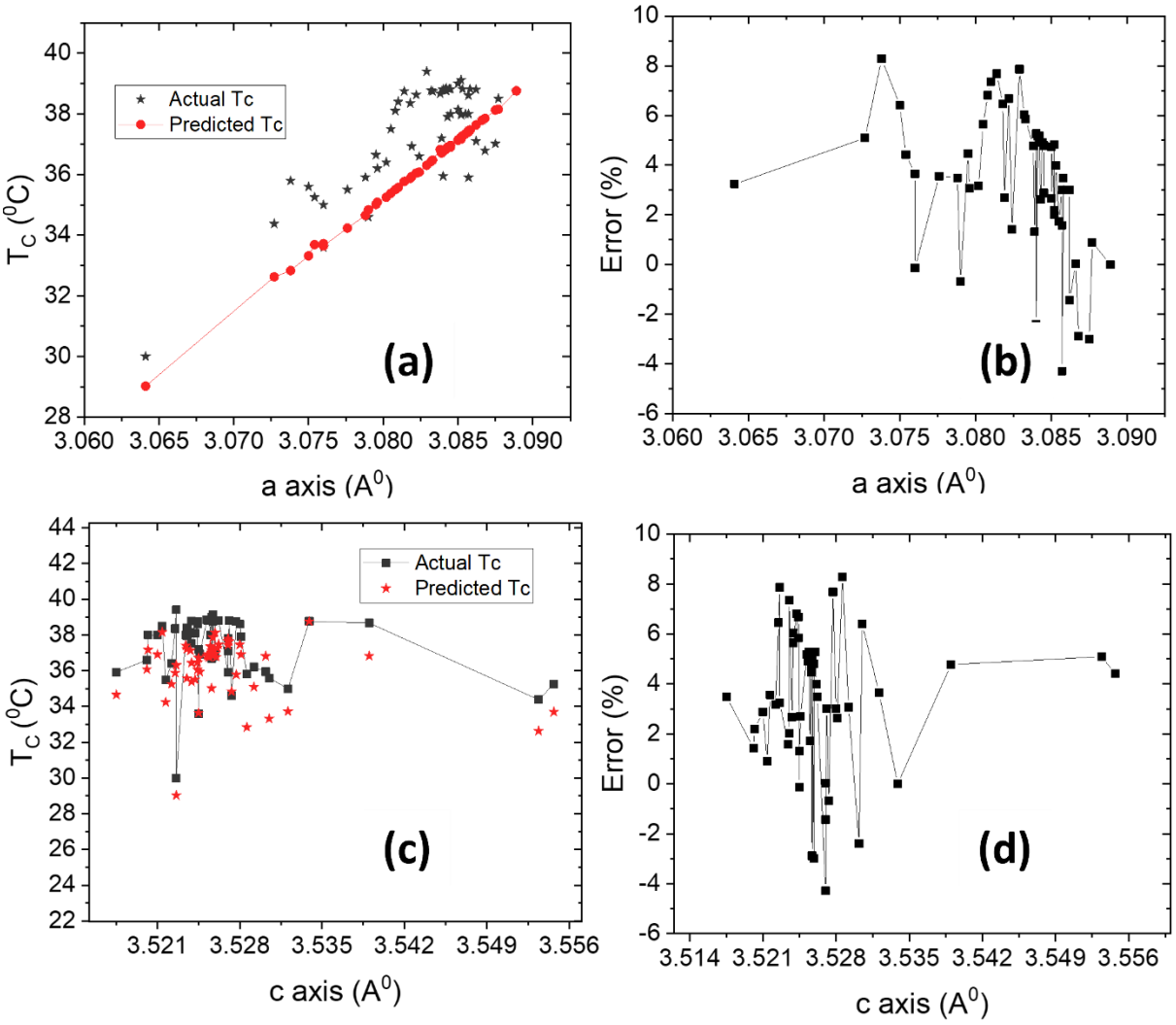

Figure 13: SVR computed dependence of T_C on lattice parameters (a) a axis relation (b) error in a axis prediction (c) c axis relation (d) error in c axis prediction.

Owing to the highest diamagnetic signal for moment measurements at different synthesis temperature for MgB_2 samples and marginal change in T_C after 1000^0C, the 1000^0C sample was chosen for further investigation using RE dopants. In order to make the choice of dopants more efficient, the SVR model was trained using data set obtained from literature for the lattice

parameters of doped MgB_2 materials. The effect of a and c axis parameters has already been explained in the sections mentioned above. SVR model was trained with sample data set of MgB_2 from experimentally verified T_C values. It was used to predict the T_C for MgB_2 materials based on lattice parameters acuqired from XRD measurements for doped and undoped samples. As given in Fig. 13 (a) to (d), the predictions were accurate for test data with an average error of +-1.26 % in T_C prediction. The model has been implemented for the lattice parameters and T_C values were acquired for variable synthesis temperature and doping measurements. Yttrium and Lanthanum were chosen as the dopant candidates due to their effective flux pinning properties and negligible change in predicted T_C for both Yttrium (37.9K) and Lanthanum (37.6K).

3.2.2. Effect of Doping on Superconductivity

As shown in Fig. 14(a), the moment measurements indicate that the intermediate region between H_{C1} and H_{C2} was observed to be fairly constant over the range of doped and undoped samples. As shown in Fig. 14(b), the T_C was found to reduce with doping in the case of La and but increase by 0.1K for Y.

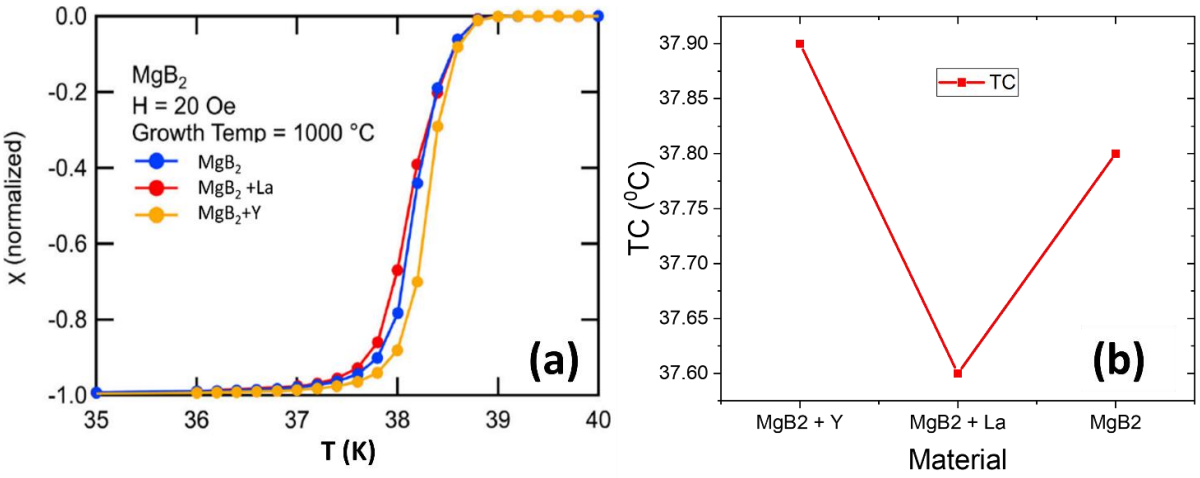

Figure 14: (a) Magnetic moment as a function temperature measurement for samples prepared at 1000^0C with La and Y doping (b) T_C for Y, La, and undoped samples.

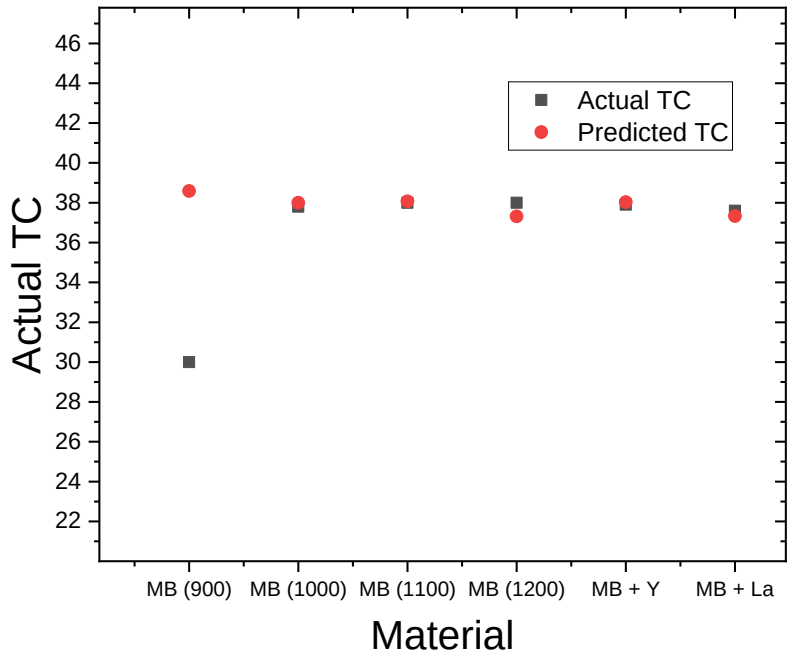

Figure 15: SVR computed T_C for all 6 samples from computed lattice parameter values.

The SVR prediction results were considerably accurate as the lattice parameter relationship predicted the T_C with reasonable precision. As shown in Fig. 15, apart from a single outlier at 900^0C, the SVR model can accurately predict the superconducting transition with a +-0.25 % error by input from the lattice parameter values.

3.2.3. Multiple Phase Formation

As shown in Fig. 16(a), weak secondary phases of Y_2O_3, La_2O_3, YB_4 and LaB_6 were observed [45]–[48]. Fig. 16(b) shows that c axis lattice parameter increases both for La and Y doped samples indicating an increase in distance between the Mg-B planes, whereas the a axis only decreases for La. The crystallite size and strain for Y doped samples was also considerably higher as compared to those observed in pure MgB_2 and La doped sample. RE elements are highly reactive in open air and when in contact with atmospheric oxygen, they readily form oxides [49]. The La and Y have a strong affinity towards negative elements such as B and O.

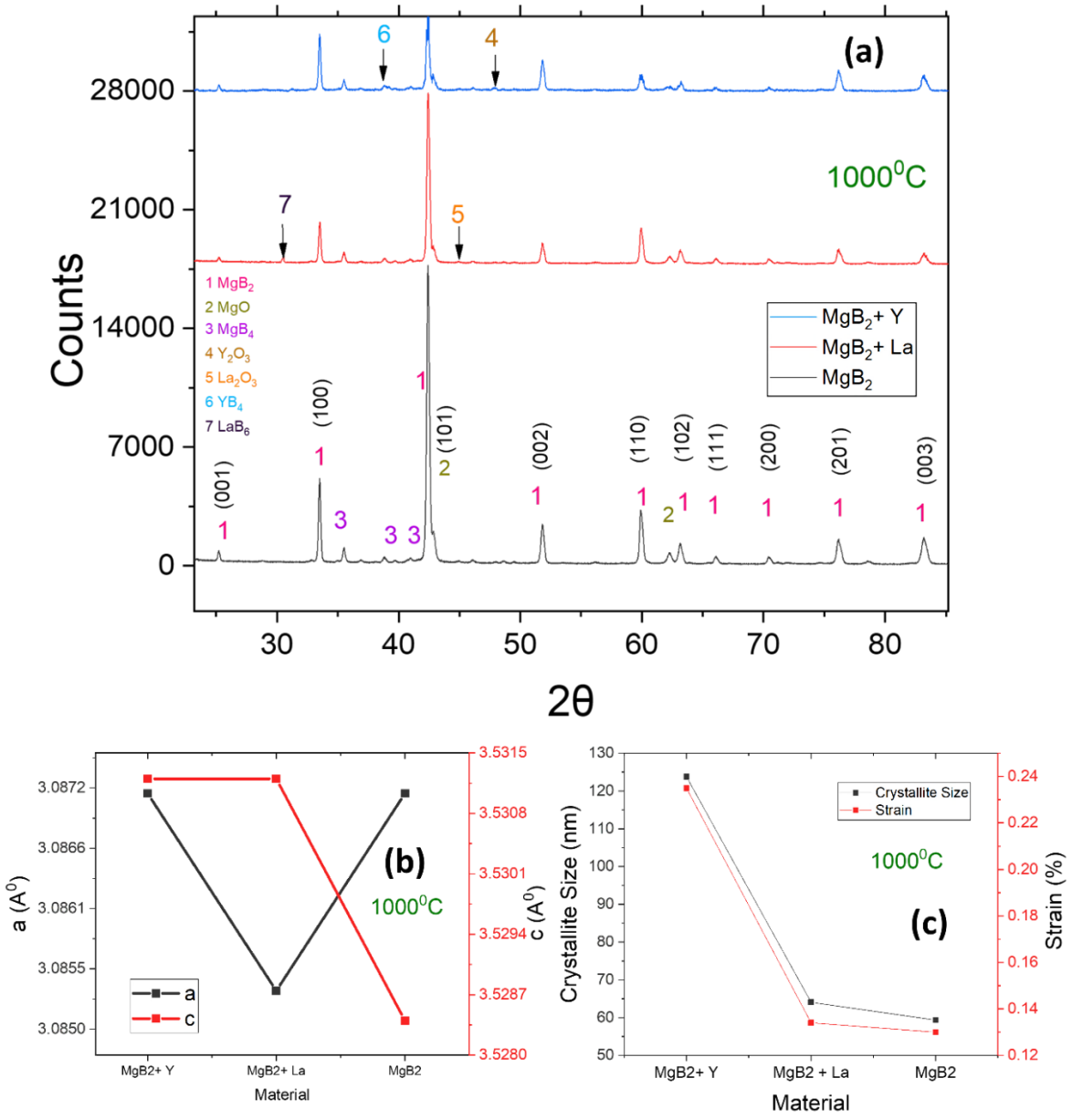

Figure 16: (a) XRD charts for undoped, Y, and La-doped samples at 1000^{0}C synthesis temperature (b) a and c axis lattice parameter for doped and undoped samples (c) Calculated crystallite size and lattice strain for doped and undoped samples.

Both La and Y are considerably large elements which on substitution in the lattice increase the distance between the c axis planes and could possibly explain the increase in crystallite size and

lattice strain. In the case of a axis, the decrease in lattice parameter is due to La substitution in the lattice as LaB_6 which has a similar coherence length as MgB_2 and therefore easily replaces Mg as a substitute. La being more electropositive than Mg tends to form stronger bonds with B and therefore reduces the a axis parameter.

3.2.4. Rare Earth Clustering

The distribution of Y and La has been studied using EDS color maps. As shown in Fig. 17(a) & (b), Y doped sample was found to have a smoother surface texture as compared to the La sample. Similar dark pits as observed in 1000 and 1100^0C samples are seen in doped samples as well.

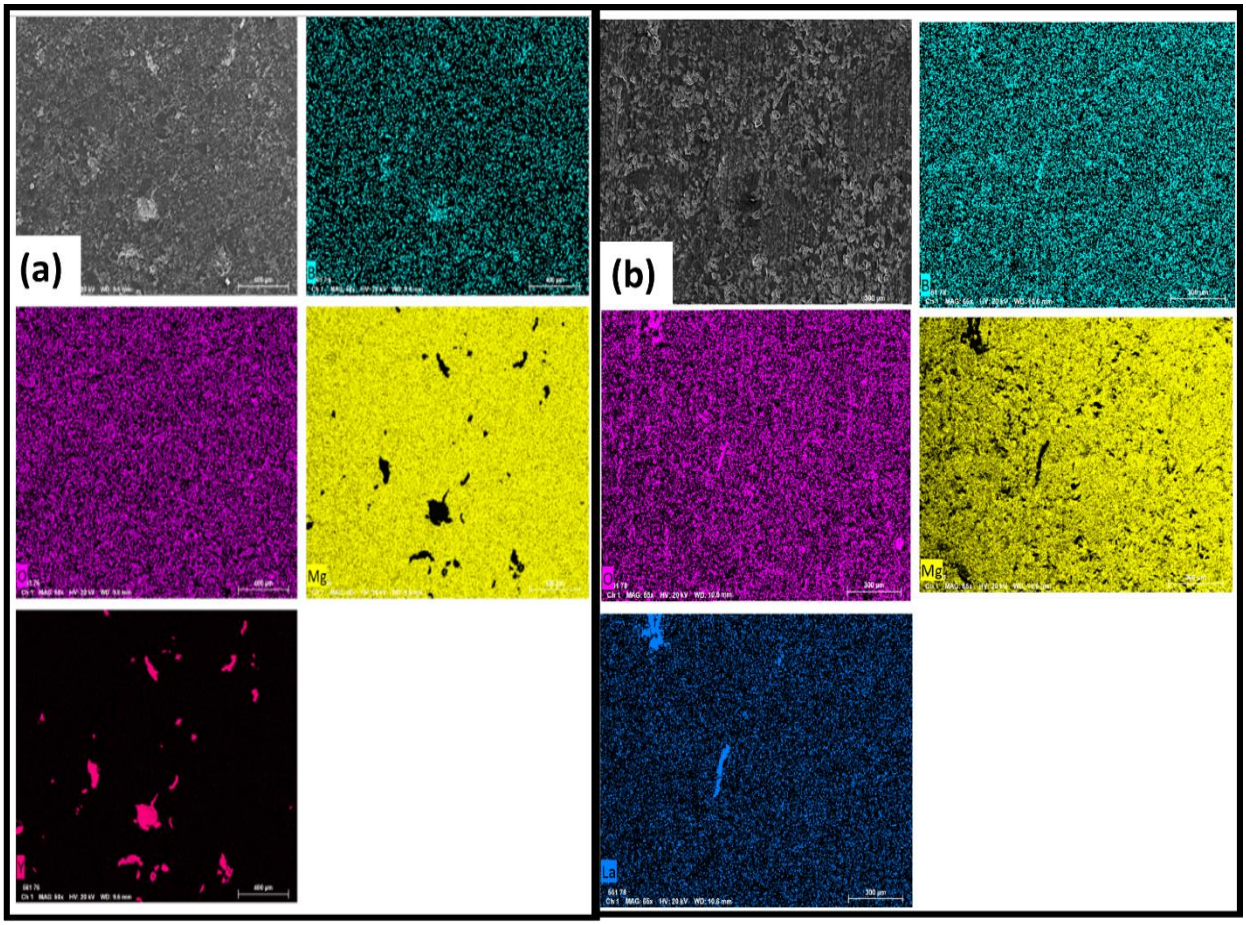

Figure 17: EDS elemental color maps for (a) Y doped (b) La-doped samples showing accumulation of RE into clusters.

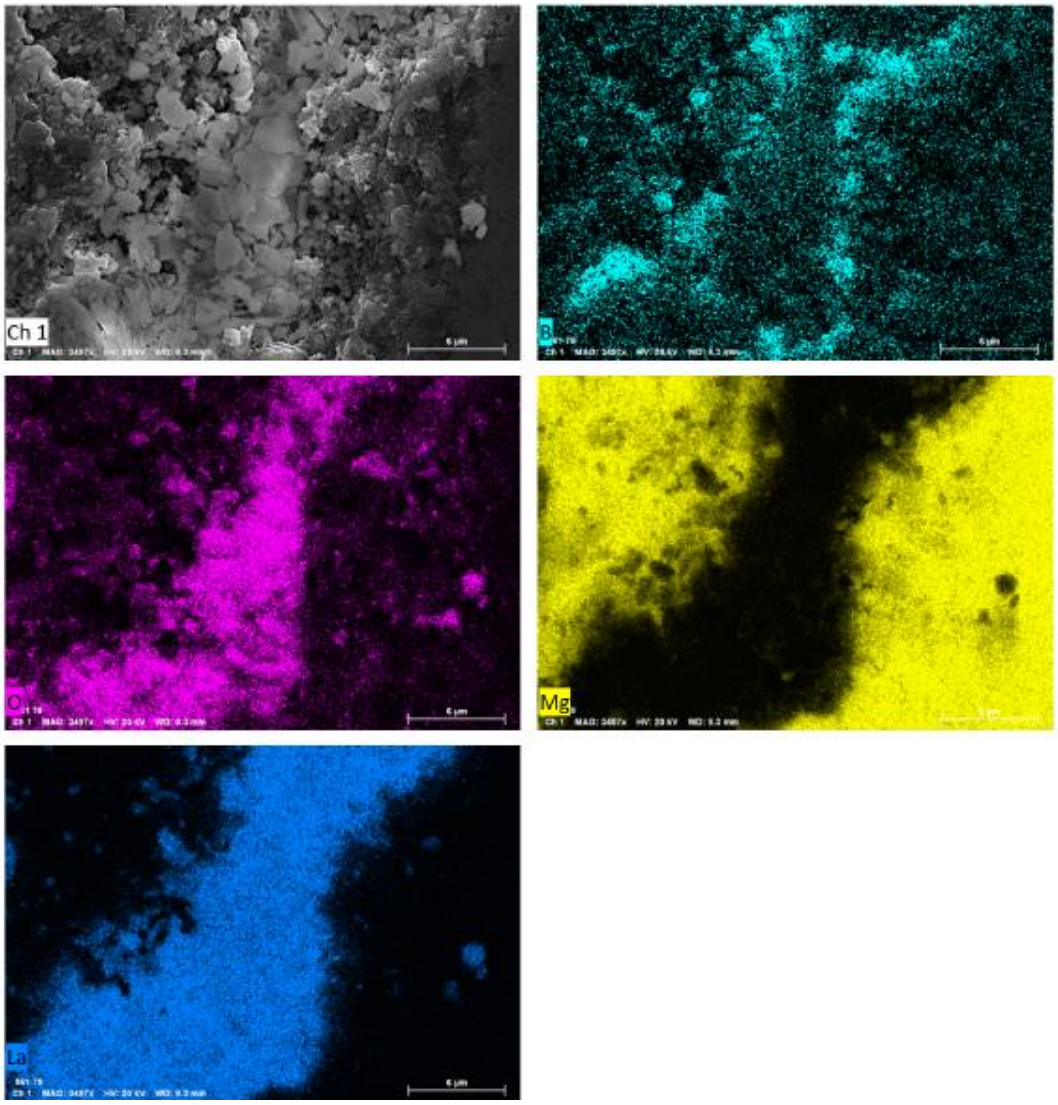

Figure 18: EDS elemental color map for La-doped sample showing Oxygen, Lanthanum, and Boron accumulation.

These dark pits are deficient in Mg and rich in La, Y and B indicate clusters of LaB_6 and YB_4 regions. The RE dopants are found to come together in clusters which show a natural tendency for segregation with the MgB_2 material when synthesized at 1000^0C. The segregated phases form long range ordered structures with B atoms as confirmed by XRD to be $P4/mbm$ & $Pm\bar{3}m$ space

groups for YB_4 and LaB_6, respectively. These RE clusters give a strong O signal as well indicating the oxide formation linked to Y_2O_3 and La_2O_3, as was observed in the XRD.

As given in Fig. 18, a detailed microstructure of the La doped region reveals how the B, O and La atoms accumulate in these LaB_6 and La_2O_3 rich zones and are sparsely distributed in the La dominated region which is in sharp contrast with Mg signal which is drastically reduced in the presence of La atoms. This confirms the hypothesis that the La atoms substitute the Mg atoms in the lattice to form a secondary phase of LaB_6.

4. Conclusions and Prospects

The effect of sintering temperature on MgB_2 bulks was studied. It was found that optical anisotropy in the material gives rise to different polarization-based effects which depend on the defect states present in the sample. A few factors which influence superconductivity in MgB_2 are its lattice parameters and in/out of plane atomic bond interactions. The superconducting properties improve with temperature but are limited once the grain growth starts to occur. Grain boundary interactions play a major in superconducting properties due to strong links between the grains. A major challenge in this regard is to develop techniques that reduce the formation of non-superconducting secondary phases. Rare earths were found to be effective tools for altering lattice parameters which in turn can be used as atomic tweezers to optimize the crystal structure of similar compounds. A marginal improvement in T_C with Y indicates that elements which form similar structures as MgB_2 and can substitute one or more atoms in the lattice can be effective dopants for improving superconducting properties. The SVR model was able to prove that lattice parameter can be used to predict T_C in MgB_2 based superconductors. New doping strategies can be devised for effectively finding new materials with improved T_C.

5. References

[1] R. de Bruyn Ouboter, "Heike Kamerlingh Onnes's Discovery of Superconductivity," *Sci. Am.*, vol. 276, no. 3, pp. 98–103, Aug. 1997.

[2] L. Bours, M. T. Mercaldo, M. Cuoco, E. Strambini, and F. Giazotto, "Unveiling mechanisms of electric field effects on superconductors by a magnetic field response," *Phys. Rev. Res.*, vol. 2, no. 3, p. 033353, Sep. 2020.

[3] D. Dew-Hughes, "The critical current of superconductors: an historical review," *Cit. Low Temp. Phys*, vol. 27, p. 713, 2001.

[4] P. Krogstrup *et al.*, "Epitaxy of semiconductor–superconductor nanowires," *Nat. Mater. 2014 144*, vol. 14, no. 4, pp. 400–406, Jan. 2015.

[5] UrayamaHatsumi *et al.*, "A New Ambient Pressure Organic Superconductor Based on BEDT-TTF with TC Higher than 10 K (TC=10.4 K)," *http://dx.doi.org/10.1246/cl.1988.55*, vol. 17, no. 1, pp. 55–58, Mar. 2006.

[6] V. M. Kovalev and I. G. Savenko, "Proposal for Plasmon Spectroscopy of Fluctuations in Low-Dimensional Superconductors," *Phys. Rev. Lett.*, vol. 124, no. 20, p. 207002, May 2020.

[7] P. W. ANDERSON, " RVB Redux: A Synergistic Theory of High T c Cuprates ," pp. 819–825, Jan. 2005.

[8] F. Wang and D.-H. Lee, "The Electron-Pairing Mechanism of Iron-Based Superconductors," *Science (80-.).*, vol. 332, no. 6026, pp. 200–204, 2011.

[9] A. P. Drozdov, M. I. Eremets, I. A. Troyan, V. Ksenofontov, and S. I. Shylin, "Conventional superconductivity at 203 kelvin at high pressures in the sulfur hydride system," *Nat. 2015 5257567*, vol. 525, no. 7567, pp. 73–76, Aug. 2015.

[10] A. P. Drozdov *et al.*, "Superconductivity at 250 K in lanthanum hydride under high pressures," *Nat. 2019 5697757*, vol. 569, no. 7757, pp. 528–531, May 2019.

[11] M. Cyrot, "Ginzburg-Landau theory for superconductors," *Reports Prog. Phys.*, vol. 36, no. 2, p. 103, Feb. 1973.

[12] J. Bardeen, L. N. Cooper, and J. R. Schrieffer, "Theory of superconductivity," *Phys. Rev.*, vol. 108, no. 5, pp. 1175–1204, Dec. 1957.

[13] R. A. Dunlap, "BCS theory," in *Electrons in Solids*, IOP Publishing, 2019, pp. 9–11.

[14] F. Gompf, W. Reichardt, H. Schober, B. Renker, and M. Buchgeister, "Lattice vibrations and electron-phonon coupling in superconducting quarternary borocarbides: An inelastic neutron-scattering investigation," *Phys. Rev. B*, vol. 55, no. 14, p. 9058, Apr. 1997.

[15] J. Nagamatsu, N. Nakagawa, T. Muranaka, Y. Zenitani, and J. Akimitsu, "Superconductivity at 39 K in magnesium diboride," *Nat. 2001 4106824*, vol. 410, no. 6824, pp. 63–64, Mar. 2001.

[16] M. Tomsic *et al.*, "Overview of MgB2 Superconductor Applications," *Int. J. Appl. Ceram.*

Technol., vol. 4, no. 3, pp. 250–259, Jul. 2007.

[17] H. DG, C. H, and J. JD, "The complex nature of superconductivity in MgB2 as revealed by the reduced total isotope effect," *Nature*, vol. 411, no. 6836, pp. 457–460, May 2001.

[18] C. Buzea and T. Yamashita, "Review of the superconducting properties of MgB2," *Supercond. Sci. Technol.*, vol. 14, no. 11, pp. R115--R146, Nov. 2001.

[19] M. Mudgel, V. P. S. Awana, H. Kishan, I. Felner, D. G. A. Alvarez, and G. L. Bhalla, "Superconductivity of various borides: The role of stretched c-parameter," *J. Appl. Phys.*, vol. 105, no. 7, p. 07E313, Mar. 2009.

[20] T. Matsushita, "Flux pinning in superconductors," *Flux Pinning Supercond.*, pp. 1–503, 2007.

[21] A. Murakami, A. Iwamoto, and J. G. Noudem, "Mechanical Properties of Bulk MgB2 Superconductors Processed by Spark Plasma Sintering at Various Temperatures," *IEEE Trans. Appl. Supercond.*, vol. 28, no. 3, pp. 1–4, Apr. 2018.

[22] F. Wang, J. Li, C. Shi, E. Liu, C. He, and N. Zhao, "Comparison of electronic structures and mechanical properties of MgAlB4, AlB2 and MgB2 using first-principles calculations," *Ceram. Int.*, vol. 46, no. 8, pp. 12548–12558, Jun. 2020.

[23] P. Bordet *et al.*, "Absence of a structural transition up to 40 GPa in MgB2," *Phys. Rev. B*, vol. 64, no. 17, p. 172502, Oct. 2001.

[24] S. K. Chen, M. Wei, and J. L. MacManus-Driscoll, "Strong pinning enhancement in MgB2 using very small Dy2O3 additions," *Appl. Phys. Lett.*, vol. 88, no. 19, p. 192512, May 2006.

[25] J. Wang *et al.*, "High critical current density and improved irreversibility field in bulk MgB2 made by a scaleable, nanoparticle addition route," *Appl. Phys. Lett.*, vol. 81, no. 11, p. 2026, Sep. 2002.

[26] J. G. Noudem, M. Aburras, P. Bernstein, X. Chaud, M. Muralidhar, and M. Murakami, "Development in processing of MgB2 cryo-magnet superconductors," *J. Appl. Phys.*, vol. 116, no. 16, p. 163916, Oct. 2014.

[27] J. G. Noudem, L. Dupont, L. Gozzelino, and P. Bernstein, "Superconducting Properties of MgB2 Bulk Shaped by Spark Plasma Sintering," *Mater. Today Proc.*, vol. 3, no. 2, pp. 545–549, Jan. 2016.

[28] Y. Guo, W. Zhang, D. Yang, and R.-L. Yao, "Decomposition and Oxidation of Magnesium Diboride," *J. Am. Ceram. Soc.*, vol. 95, no. 2, pp. 754–759, Feb. 2012.

[29] Z. A. Munir, U. Anselmi-Tamburini, and M. Ohyanagi, "The effect of electric field and pressure on the synthesis and consolidation of materials: A review of the spark plasma sintering method," *J. Mater. Sci. 2006 413*, vol. 41, no. 3, pp. 763–777, Feb. 2006.

[30] M. Awad and R. Khanna, "Support Vector Regression," in *Efficient Learning Machines*, M. Awad and R. Khanna, Eds. Berkeley, CA: Apress, 2015, pp. 67–80.

[31] V. Cherkassky and F. Mulier, "Vapnik-Chervonenkis (VC) learning theory and its

applications," *IEEE Trans. Neural Networks*, vol. 10, no. 5, pp. 985–987, 1999.

[32] C. Z. Cai, G. L. Wang, Y. F. Wen, J. F. Pei, X. J. Zhu, and W. P. Zhuang, "Superconducting Transition Temperature Tc Estimation for Superconductors of the Doped MgB2 System Using Topological Index via Support Vector Regression," *J. Supercond. Nov. Magn. 2010 235*, vol. 23, no. 5, pp. 745–748, Jan. 2010.

[33] A. Khorsand Zak, W. H. Abd. Majid, M. E. Abrishami, and R. Yousefi, "X-ray analysis of ZnO nanoparticles by Williamson–Hall and size–strain plot methods," *Solid State Sci.*, vol. 13, no. 1, pp. 251–256, Jan. 2011.

[34] R. Wirth, "Focused Ion Beam (FIB) combined with SEM and TEM: Advanced analytical tools for studies of chemical composition, microstructure and crystal structure in geomaterials on a nanometre scale," *Chem. Geol.*, vol. 261, no. 3–4, pp. 217–229, Apr. 2009.

[35] V. Guritanu, A. B. Kuzmenko, D. van der Marel, S. M. Kazakov, N. D. Zhigadlo, and J. Karpinski, "Anisotropic optical conductivity and two colors of MgB2," *Phys. Rev. B*, vol. 73, no. 10, p. 104509, Mar. 2006.

[36] O. Loebich, "The optical properties of gold," *Gold Bull. 1972 51*, vol. 5, no. 1, pp. 2–10, Mar. 1972.

[37] Y. Fudamoto and S. Lee, "Anisotropic electrodynamics of MgB2 detected by optical reflectance," *Phys. Rev. B*, vol. 68, no. 18, p. 184514, Nov. 2003.

[38] J. Bardeen, "Theory of the Meissner Effect in Superconductors," *Phys. Rev.*, vol. 97, no. 6, p. 1724, Mar. 1955.

[39] unicated F. by A Lindemann, "The electromagnetic equations of the supraconductor," *Proc. R. Soc. London. Ser. A - Math. Phys. Sci.*, vol. 149, no. 866, pp. 71–88, Mar. 1935.

[40] A. A. Abrikosov, "The magnetic properties of superconducting alloys," *J. Phys. Chem. Solids*, vol. 2, no. 3, pp. 199–208, Jan. 1957.

[41] L.-H. He, G.-Q. Hu, P.-L. Zhang, and Q.-W. Yan, "Structure analysis of new superconductor Mg B2," *Chinese Phys.*, vol. 10, pp. 343–344, 2001.

[42] M. I. McCarthy and N. M. Harrison, "Ab initio determination of the bulk properties of Mg O," *Phys. Rev. Ser. 3. B - Condens. Matter*, vol. 49, pp. 8574–8582, 1994.

[43] W. L. Bragg, "Crystal structure," *Nat.*, vol. 105, pp. 646–648, 1920.

[44] S. E. Babcock and J. L. Vargas, "THE NATURE OF GRAIN BOUNDARIES IN THE HIGH-Tc SUPERCONDUCTORS," *Annu. Rev. Mater. Sci*, vol. 25, pp. 193–222, 1995.

[45] M. S. Babu *et al.*, "Enhanced photoelectrochemical water splitting behaviour of tuned band gap CdSe QDs sensitized LaB6," *J. Nanosci. Nanotechnol.*, vol. 17, no. 1, pp. 437–442, 2017.

[46] H. Kabir, S. H. Nandyala, M. M. Rahman, M. A. Kabir, and A. Stamboulis, "Influence of calcination on the sol–gel synthesis of lanthanum oxide nanoparticles," *Appl. Phys. A 2018 12412*, vol. 124, no. 12, pp. 1–11, Nov. 2018.

[47] K. Jayasankar, A. Pandey, B. K. Mishra, and S. Das, “Evaluation of microstructural parameters of nanocrystalline Y2O3 by X-ray diffraction peak broadening analysis,” *Mater. Chem. Phys.*, vol. 171, pp. 195–200, Mar. 2016.

[48] R. M. Da Rocha and F. C. L. De Melo, “Sintering of B4C by pressureless liquid phase sintering,” *Mater. Sci. Forum*, vol. 660–661, pp. 170–175, 2010.

[49] G. Borzone, R. Raggio, and R. Ferro, “Thermochemistry and reactivity of rare earth metals,” *Phys. Chem. Chem. Phys.*, vol. 1, no. 7, pp. 1487–1500, Jan. 1999.